Structural Influences of Organonitrogen Ligands on Vanadium Oxide Solids. Hydrothermal Syntheses and Structures of the Terpyridine Vanadates $[V_2O_4(Terpy)_2]_3[V_{10}O_{28}]$, $[VO_2(Terpy)][V_4O_{10}]$, and $[V_9O_{22}(Terpy)_3]$

Pamela J. Hagrman and Jon Zubieta*

Department of Chemistry, Syracuse University, Syracuse, New York 13244

Received December 22, 1999

Hydrothermal reactions of the V_2O_5/2,2′:6′:2″-terpyridine/ZnO/H_2O system under a variety of conditions yielded the organic−inorganic hybrid materials $[V_2O_4(terpy)_2]_3[V_{10}O_{28}]\cdot 2H_2O$ (**VOXI-10**), $[VO_2(terpy)][V_4O_{10}]$ (**VOXI-11**), and $[V_9O_{22}(terpy)_3]$ (**VOXI-12**). The structure of **VOXI-10** consists of discrete binuclear cations $[V_2O_4(terpy)_2]^{2+}$ and one-dimensional chains $[V_{10}O_{28}]^{6-}$, constructed of cyclic $[V_4O_{12}]^{4-}$ clusters linked through $\{VO_4\}$ tetrahedra. In contrast, the structure of **VOXI-11** exhibits discrete mononuclear cations $[VO_2(terpy)]^{1+}$ and a two-dimensional vanadium oxide network, $[V_4O_{10}]^{1-}$. The structure of the oxide layer is constructed from ribbons of edge-sharing square pyramids; adjacent ribbons are connected through corner-sharing interactions into the two-dimensional architecture. **VOXI-12** is also a network structure; however, in this case the terpy ligand is incorporated into the two-dimensional oxide network whose unique structure is constructed from cyclic $[V_6O_{18}]^{6-}$ clusters and linear $\{V_3O_5(terpy)_3\}$ moieties of corner-sharing vanadium octahedra. The rings form chains through corner-sharing linkages; adjacent chains are connected through the trinuclear units. Crystal data: **VOXI-10**, $C_{90}H_{70}N_{18}O_{42}V_{16}$, triclinic $P\bar{1}$, $a = 12.2071(7)$ Å, $b = 13.8855(8)$ Å, 16.9832(10) Å, $\alpha = 69.584(1)°$, $\beta = 71.204(1)°$, $\gamma = 84.640(1)°$, $Z = 1$; **VOXI-11**, $C_{15}H_{11}N_3O_{12}V_5$, monoclinic, $P2_1/n$, $a = 7.7771(1)$ Å, $b = 10.3595(2)$ Å, $c = 25.715(4)$ Å, $\beta = 92.286(1)°$, $Z = 4$; **VOXI-12**, $C_{45}H_{33}N_9O_{22}V_9$, monoclinic $C2/c$, $a = 23.774(2)$ Å, $b = 9.4309(6)$ Å, $c = 25.380(2)$ Å, $\beta = 112.047(1)°$, $Z = 4$.

The role of organic components in the structural modification of inorganic oxides[1,2] has been extensively documented in recent years for zeolites,[3,4] mesoporous materials of the MCM-41 class,[5] transition metal phosphates,[6,7] and the products of biomineralization.[8−10] More recently, the emerging chemistry of organic-directed crystallization of molybdenum oxides has been reviewed.[11,12] While the organic structure-directing component of such hybrid materials is conventionally introduced as a charge-compensating and space-filling constituent, it may also function as a ligand, coordinated directly to the oxide scaffolding or to a secondary metal center. The ligand may thus function to "passivate" the surface of the growing oxide by coordination to the metal centers or, in the case of bridging groups, to transmit spatially the structural information inherent in the coordination preferences of a particular transition metal center. Passivation of the metal oxide coordination sphere, in the sense of blocking further metal−oxo bond formation, is illustrated by the structures of the family of hybrid materials $[(MoO_3)_n(2,2'\text{-bipy})_m]$,[13] while the exploitation of the ligand geometry in the spatial transmission of structural information is exemplified by the structures of [Cu(4,4′-bipyridylamine)MoO_4],[14] [{Cu_2 (triazolate)$_2(H_2O)_2$}Mo_4O_{13}],[15] and [Cu(tetrapyridylporphyrin)$Cu_2Mo_3O_{11}$].[16]

The expansion of hybrid organic−metal oxide chemistry to the vanadium oxides has largely focused on layered vanadium oxides with interlayer organic cations[17−29] and metal coordina-

(1) Stupp, S. I.; Braun, P. V. *Science* **1997**, *277*, 1242.
(2) Braun, P. V.; Osenar, P.; Tohver, V.; Kennedy, S. B.; Stupp, S. I. *J. Am. Chem. Soc.* **1999**, *121*, 7302.
(3) Vaughan, D. E. W. *Properties and Applications of Zeolites* (Chemical Society Special Publication No. 33); Townsend, R. P., Ed.; The Chemical Society: London, 1979; p 294.
(4) Davis, M. E.; Lobo, R. F. *Chem. Mater.* **1992**, *4*, 756.
(5) Kresge, C. T.; Leonowicz, M. E.; Roth, W. J.; Vartuli, J. C.; Beck, J. S. *Nature* **1992**, *359*, 710.
(6) Khan, M. I.; Meyer, L. M.; Haushalter, R. C.; Sweitzer, C. L.; Zubieta, J.; Dye, J. L. *Chem. Mater.* **1996**, *8*, 43.
(7) Feng, P.; Bu, X.; Stucky, G. D. *Nature* **1997**, *388*, 735.
(8) Mann, S. *Nature* **1993**, *365*, 499.
(9) Mann, S.; Burkett, S. L.; Davis, S. A.; Fowler, C. E.; Mendelson, N. H.; Sims, S. D.; Walsh, D.; Whilton, N. T. *Chem. Mater.* **1997**, *9*, 2300.
(10) Li, M.; Wong, K. K. W.; Mann, S. *Chem. Mater.* **1999**, *11*, 23.
(11) Hagrman, P. J.; Hagrman, D.; Zubieta, J. *Angew. Chem., Int. Ed. Engl.* **1999**, *38*, 2638.
(12) Chesnut, D. J.; Hagrman, D.; Zapf, P. J.; Hammond, R. P.; LaDuca, R.; Haushalter, R. C.; Zubieta, J. *Coord. Chem. Rev.* **1999**, *190−192*, 737.
(13) Zapf, P. J.; Haushalter, R. C.; Zubieta, J. *Chem. Mater.* **1997**, *9*, 2019.
(14) Hagrman, D.; Warren, C. J.; Haushalter, R. C.; Seip, C.; O'Connor, C. J.; Rarig, R. S., Jr.; Johnson, K. M., III; LaDuca, R. L., Jr.; Zubieta, J. *Chem. Mater.* **1998**, *10*, 3294.
(15) Hagrman, D.; Zubieta, J. *Chem. Commun.* **1998**, 2005.
(16) Hagrman, D.; Hagrman, P. J.; Zubieta, J. *Angew. Chem., Int. Ed. Engl.*, in press.
(17) Zhang, Y.; O'Connor, C. J.; Clearfield, A.; Haushalter, R. C. *Chem. Mater.* **1996**, *8*, 595.
(18) Riou, D.; Férey, G. *J. Solid State Chem.* **1995**, *120*, 137.
(19) Riou, D.; Férey, G. *Inorg. Chem.* **1995**, *34*, 6520.
(20) Riou, D.; Férey, G. *J. Solid State Chem.* **1995**, *124*, 151.
(21) Chirayil, T. G.; Boylan, E. A.; Mamak, M.; Zavalij, P. Y.; Whittingham, M. S. *Chem. Commun.* **1997**, 33.
(22) Zhang, Y.; Haushalter, R. C.; Clearfield, A. *Chem. Commun.* **1996**, 1055.
(23) Zhang, Y.; Warren, C. J.; Haushalter, R. C. *Chem. Mater.* **1998**, *10*, 1059.
(24) Nazar, L. F.; Koene, B. E.; Britten, J. F. *Chem. Mater.* **1996**, *8*, 327.
(25) Shan, Y.; Huang, R. H.; Huang, S. D. *Angew. Chem., Int. Ed. Engl.* **1999**, *38*, 1751.
(26) Koene, B. E.; Taylor, N. J.; Nazar, L. F. *Angew. Chem., Int. Ed. Engl.* **1999**, *38*, 2888.

10.1021/ic991473d CCC: $19.00
Published on Web 06/27/2000

tion complexes[30] and one- and two-dimensional vanadium oxide substructures decorated with or linked by secondary-metal ligand complexes.[30−32] In contrast, vanadium oxide phases incorporating ligands coordinated directly to the vanadium sites of the oxide scaffolding have not been systematically studied. However, the dramatic influence of organic components on oxide microstructure is apparent in the structures of the one-dimensional $[V_9O_{21}(bpy)_4]$[33] and the two-dimensional $[V_3O_7(o\text{-phen})]$[34] and $[VF(PO_4)(H_2NCH_2CH_2NH_2)]$.[35] As part of our continuing studies of the structure-directing role of ligands in metal oxide phases, we have sought to expand these previous studies of prototypical structures to the vanadium oxide−terpyridyl system. The hydrothermal syntheses and structures of three novel vanadium oxides are reported: the one-dimensional $[V_2O_4(terpy)_2]_3[V_{10}O_{28}]$ (**VOXI-10**), the two-dimensional $[VO_2(terpy)][V_4O_{10}]$ (**VOXI-11**), and the two-dimensional $[V_9O_{22}(terpy)_3]$ (**VOXI-12**).

Experimental Section

Reagents were purchased from Aldrich Chemical Co. and used without further purification. All syntheses were carried out in 23 mL poly(tetrafluoroethylene)-lined stainless steel containers under autogenous pressure. The reactants were stirred briefly before heating. Water was distilled above 3.0 Ω in-house using a Barnstead model 525 Biopure distilled water center.

Synthesis of $[V_2O_4(terpy)_2]_3[V_{10}O_{28}]\cdot 2H_2O$ (VOXI-10). A mixture of V_2O_5 (0.1057 g), 2,2′:6′,2″-terpyridine (0.1368 g), ZnO (0.0235 g), and H_2O (8.0394 g) in the mole ratio 1:1:0.5:770 was heated for 6 days at 210 °C. Yellow crystals of **VOXI-10** were isolated in 20% yield by mechanical separation from an orange amorphous solid. Anal. Calcd for $C_{45}H_{35}N_9O_{21}V_8$: C, 37.4; H, 2.42; N, 8.72. Found: C, 37.1; H, 2.55; N, 8.65.

Synthesis of $[VO_2(terpy)][V_4O_{10}]$ (VOXI-11) and $[V_9O_{22}(terpy)_3]$ (VOXI-12). A mixture of V_2O_5 (0.1055 g), 2,2′:6′:2″-terpyridine (0.1356 g), ZnO (0.0242 g), and H_2O (8.0355 g) in the mole ratio 1:1:0.5:770 was heated at 210 °C for 8 days. After the mixture was cooled to room temperature, rootbeer-colored blocks of **VOXI-11** were separated mechanically from dark blue-black plates of **VOXI-12**. The yields were ca. 15% and 25%, respectively, based on vanadium. Anal. Calcd for $C_{15}H_{11}N_3O_{12}V_5$ (**VOXI-11**): C, 26.5; H, 1.62; N, 6.18. Found: C, 26.7; H, 1.55; N, 6.35. Calcd for $C_{45}H_{33}N_9O_{22}V_9$ (**VOXI-12**): C, 35.7; H, 2.19; N, 8.35. Found: C, 35.8; H, 2.01; N, 8.07.

X-ray Crystallography. Structural measurements for **VOXI-10−12** were performed on a Bruker SMART-CCD diffractometer at a temperature of 150 ± 1 K using graphite monochromated Mo Kα radiation (λ(Mo Kα) = 0.710 73 Å). The data were corrected for Lorentz and polarization effects and absorption using SADABS. The structures were solved by direct methods.[36] In all cases, all non-hydrogen atoms were refined anistropically. Neutral atom scattering coefficients and anomalous dispersion corrections were taken from the International Tables, Volume C.[37] All calculations were performed using the SHELXTL[38] crystallographic software packages.

Crystallographic details for the structures of **VOXI-10−12** are summarized in Table 1. Atomic positional parameters, tables of bond lengths and angles, and anisotropic temperature factors are available in Supporting Information. Selected bond lengths and angles for **VOXI-10**, **-11,** and **-12** are given in Tables 2, 3, and 4, respectively.

Table 1. Summary of Crystallographic Data for the Structures of $[V_2O_4(terpy)_2]_3[V_{10}O_{28}]\cdot 2H_2O$ (**VOXI-10**), $[VO_2(terpy)][V_4O_{10}]$ (**VOXI-11**), and $[V_9O_{22}(terpy)_3]$ (**VOXI-12**)

	VOXI-10	VOXI-11	VOXI-12
empirical formula	$C_{45}H_{35}N_9O_{21}V_8$	$C_{15}H_{11}N_3O_{12}V_5$	$C_{45}H_{33}N_9O_{22}V_9$
fw	1445.34	679.97	1510.27
space group	$P\bar{1}$ (No. 2)	$P2_1/n$ (No. 14)	$C2/c$ (No. 15)
a, Å	12.2071(7)	7.7771(1)	23.774(2)
b, Å	13.8855(8)	10.3595(2)	9.4309(6)
c, Å	16.983(1)	25.7150(4)	25.380(2)
α, deg	69.584(1)	90.0	90.0
β, deg	71.204(1)	92.286(1)	112.047(1)
γ, deg	84.640(1)	90.0	90.0
vol, Å^3	2553.4(3)	2070.13(6)	5274.3(6)
Z	2	4	4
D_{calc}, g cm^{-3}	1.880	2.182	1.902
μ, mm^{-1}	1.488	2.247	1.610
temp, K	96	96	96
λ, Å	0.710 73	0.710 73	0.710 73
R1[a]	0.0569	0.0636	0.0383
wR2[b]	0.1095	0.0962	0.0765

[a] $R1 = \sum||F_o| - |F_c||/\sum|F_o|$. [b] $wR2 = \{\sum(w(F_o^2 - F_c^2)^2/\sum(w(F_o^2)^2)\}^{1/2}$.

Results and Discussion

The isolation of **VOXI-10−12** relies on hydrothermal techniques.[39−41] While hydrothermal synthesis has been long employed in the preparation of zeolites,[42] the method has only recently been applied to the synthesis of other organic−inorganic hybrid materials. However, given the extensive use of hydrothermal methods in the preparation of molybdenum oxides,[11,12,43] metal halide and pseudohalide phases,[44,45] and metal phosphate and phosphonate materials,[6,7,46] this can no longer be considered a recondite approach to the isolation of new materials. Hydrothermal synthesis exploits the reduced viscosity of water at temperatures above 100 °C and autogenous pressure to promote solvent extraction of solids and crystal growth from solution. Another advantage of the method for the preparation of hybrid materials is the ready solubilization of both organic and inorganic starting materials, which alleviates differential solubility problems. The working temperature range of 120−250 °C, in contrast to the elevated temperatures of conventional solid-

(27) Zhang, Y.; Haushalter, R. C.; Clearfield, A. *Inorg. Chem.* **1996**, *35*, 4950.
(28) Whittingham, M. S.; Guo, J.-D.; Chen, R.; Chirayil, T.; Janauer, G.; Zavalij, P. *Solid State Ionics* **1995**, *75*, 257.
(29) Chirayil, T.; Zavalij, R. Y.; Whittingham, M. S. *Chem. Mater.* **1998**, *10*, 2629.
(30) Zhang, Y.; DeBord, J. R. D.; O'Connor, C. J.; Haushalter, R. C.; Clearfield, A.; Zubieta, J. *Angew. Chem., Int. Ed. Engl.* **1996**, *35*, 989.
(31) LaDuca, R. L., Jr.; Finn, R.; Zubieta, J. *Chem. Commun.* **1999**, 1669.
(32) Hagrman, P. J.; Bridges, C.; Greedan, J. E.; Zubieta, J. *J. Chem. Soc., Dalton Trans.* **1999**, 2901.
(33) Huan, G.; Johnson, J. W.; Jacobsen, G. J.; Merola, J. S. *J. Solid State Chem.* **1991**, *91*, 385.
(34) Duan, C.-Y.; Tian, Y.-P.; Lu, Z.-L.; You, X.-Z. *Inorg. Chem.* **1995**, *34*, 1.
(35) Riou-Cavallec, M.; Serre, C.; Férey, G. *C. R. Acad. Sci. Paris, Ser. IIC* **1999**, *2*, 147.
(36) *SHELXTL PC*; Siemens Analytical X-ray Instruments: Madison, WI, 1993.
(37) *International Tables for Crystallography*; Volume C, Tables 4.2.6.8 and 6.1.1.4.
(38) Sheldrick, G. M. *SHELXTL. Structure Determination Programs*, version 5.0; PC Siemens Analytical Systems: Madison, WI, 1994.
(39) Rabenau, A. *Angew. Chem., Int. Ed. Engl.* **1985**, *24*, 1026.
(40) Laudise, R. A. *Chem. Eng. News* **1987**, Sep 28, 30.
(41) Gopalakrishnan, J. *Chem. Mater.* **1995**, *7*, 1265.
(42) Barrer, R. M. *Hydrothermal Chemistry of Zeolites*; Academic Press: New York, 1982.
(43) Hagrman, D.; Zubieta, J. *Trans. Am. Crystallogr. Assoc.* **1998**, *33*, 109.
(44) (a) Francis, R. J.; Halasyamani, P. S.; O'Hare, D. *Angew. Chem., Int. Ed. Engl.* **1998**, *37*, 2214. (b) Mitzi, D. *Chem. Mater.* **1996**, *8*, 791. (c) DeBord, J. R. D.; Lu, Y.-J.; Warren, C. J.; Haushalter, R. C.; Zubieta, J. *Chem. Commun.* **1997**, 1365.
(45) (a) Chesnut, D. J.; Kusnetzow, A.; Zubieta, J. *J. Chem. Soc., Dalton Trans.* **1998**, 4081. (b) Chesnut, D. J.; Zubieta, J. *Chem. Commun.* **1998**, 1707. (c) Chestnut, D. J.; Kuznetzow, A.; Birge, R. R.; Zubieta, J. *Inorg. Chem.* **1999**, *38*, 2663.
(46) Khan, M. I.; Zubieta, J. *Prog. Inorg. Chem.* **1995**, *43*, 1.

Table 2. Selected Bond Lengths (Å) and Angles (deg) for $[V_2O(terpy)_2]_3[V_{10}O_{28}]\cdot 2H_2O$ (**VOXI-10**)[a]

V(1)−O(1)	1.606(3)	V(4)−O(9)	1.844(3)
V(1)−O(2)	1.657(3)	V(4)−O(11)#1	1.848(3)
V(1)−N(1)	2.089(3)	V(5)−O(10)	1.605(3)
V(1)−N(3)	2.093(3)	V(5)−O(12)	1.739(3)
V(1)−N(2)	2.120(3)	V(5)−O(11)	1.748(3)
V(2)−O(3)	1.600(3)	V(5)−O(9)	1.774(3)
V(2)−O(4)	1.669(3)	V(6)−O(13)	1.626(3)
V(2)−N(6)	2.103(3)	V(6)−O(14)	1.631(3)
V(2)−N(4)	2.107(3)	V(6)−O(12)	1.825(3)
V(2)−N(5)	2.136(3)	V(6)−O(15)	1.846(3)
V(2)−O(5)	2.318(3)	V(7)−O(17)	1.611(3)
V(3)−O(6)	1.600(3)	V(7)−O(15)	1.750(3)
V(3)−O(5)	1.665(3)	V(7)−O(18)	1.751(3)
V(3)−N(7)	2.101(3)	V(7)−O(16)	1.755(3)
V(3)−N(9)	2.104(3)	V(8)−O(19)	1.625(3)
V(3)−N(8)	2.128(3)	V(8)−O(20)	1.632(3)
V(3)−O(4)	2.343(3)	V(8)−O(18)	1.834(3)
V(4)−O(7)	1.623(3)	V(8)−O(16)#2	1.834(3)
V(4)−O(8)	1.632(3)		

O(1)−V(1)−O(2)	106.54(15)	N(8)−V(3)−O(4)	72.58(12)
O(1)−V(1)−N(1)	96.96(14)	O(7)−V(4)−O(8)	108.11(16)
O(2)−V(1)−N(1)	101.79(14)	O(7)−V(4)−O(9)	109.44(15)
O(1)−V(1)−N(3)	94.81(14)	O(8)−V(4)−O(9)	112.26(15)
O(2)−V(1)−N(3)	102.09(14)	O(7)−V(4)−O(11)#1	109.67(15)
N(1)−V(1)−N(3)	149.06(14)	O(8)−V(4)−O(11)#1	108.78(15)
O(1)−V(1)−N(2)	107.44(14)	O(9)−V(4)−O(11)#1	108.55(14)
O(2)−V(1)−N(2)	146.02(14)	O(10)−V(5)−O(12)	108.99(16)
N(1)−V(1)−N(2)	74.24(13)	O(10)−V(5)−O(11)	109.56(16)
N(3)−V(1)−N(2)	74.95(13)	O(12)−V(5)−O(11)	111.47(15)
O(3)−V(2)−O(4)	105.12(15)	O(10)−V(5)−O(9)	109.59(17)
O(3)−V(2)−N(6)	94.93(14)	O(12)−V(5)−O(9)	108.19(15)
O(4)−V(2)−N(6)	102.81(14)	O(11)−V(5)−O(9)	109.01(15)
O(3)−V(2)−N(4)	94.39(14)	O(13)−V(6)−O(14)	108.44(16)
O(4)−V(2)−N(4)	103.51(14)	O(13)−V(6)−O(12)	108.02(15)
N(6)−V(2)−N(4)	148.64(14)	O(14)−V(6)−O(12)	113.04(15)
O(3)−V(2)−N(5)	105.78(14)	O(13)−V(6)−O(15)	109.17(14)
O(4)−V(2)−N(5)	149.10(14)	O(14)−V(6)−O(15)	106.96(15)
N(6)−V(2)−N(5)	74.39(13)	O(12)−V(6)−O(15)	111.14(14)
N(4)−V(2)−N(5)	74.26(13)	O(17)−V(7)−O(15)	108.68(15)
O(3)−V(2)−O(5)	177.22(13)	O(17)−V(7)−O(18)	109.32(15)
O(4)−V(2)−O(5)	77.59(12)	O(15)−V(7)−O(18)	109.97(14)
N(6)−V(2)−O(5)	84.99(12)	O(17)−V(7)−O(16)	107.99(15)
N(4)−V(2)−O(5)	84.30(12)	O(15)−V(7)−O(16)	109.05(15)
N(5)−V(2)−O(5)	71.52(12)	O(18)−V(7)−O(16)	111.76(15)
O(6)−V(3)−O(5)	104.27(14)	O(19)−V(8)−O(20)	109.21(16)
O(6)−V(3)−N(7)	94.43(14)	O(19)−V(8)−O(18)	110.94(15)
O(5)−V(3)−N(7)	102.60(14)	O(20)−V(8)−O(18)	110.16(15)
O(6)−V(3)−N(9)	93.93(14)	O(19)−V(8)−O(16)#2	107.28(15)
O(5)−V(3)−N(9)	103.86(14)	O(20)−V(8)−O(16)#2	110.92(16)
N(7)−V(3)−N(9)	149.28(14)	O(18)−V(8)−O(16)#2	108.29(14)
O(6)−V(3)−N(8)	106.24(14)	V(2)−O(4)−V(3)	102.18(13)
O(5)−V(3)−N(8)	149.49(14)	V(3)−O(5)−V(2)	103.31(13)
N(7)−V(3)−N(8)	74.71(13)	V(5)−O(9)−V(4)	126.97(17)
N(9)−V(3)−N(8)	74.57(13)	V(5)−O(11)−V(4)#1	145.73(18)
O(6)−V(3)−O(4)	178.45(13)	V(5)−O(12)−V(6)	159.0(2)
O(5)−V(3)−O(4)	76.92(12)	V(7)−O(15)−V(6)	137.12(17)
N(7)−V(3)−O(4)	86.25(12)	V(7)−O(16)−V(8)#2	140.61(19)
N(9)−V(3)−O(4)	84.80(12)	V(7)−O(18)−V(8)	158.1(2)

[a] Symmetry transformations used to generate equivalent atoms: (#1) $-x+1, -y+1, -z$; (#2) $-x, -y, -z+1$.

Table 3. Selected Bond Lengths (Å), Valence Sums, and Angles (deg) for $[VO_2(terpy)][V_4O_{10}]$ (**VOXI-11**)[a]

V(1)−O(1)	1.617(3)	V(4)−O(10)	1.604(3)
V(1)−O(2)	1.619(3)	V(4)−O(3)#3	1.711(3)
V(1)−N(2)	2.101(3)	V(4)−O(7)	1.900(3)
V(1)−N(3)	2.102(3)	V(4)−O(9)#4	1.936(3)
V(1)−N(1)	2.108(3)	V(4)−O(11)	2.088(2)
		V(4)−V(5)	3.0118(8)
V(2)−O(5)	1.594(3)	Σs[V(4)−O] = 4.81	
V(2)−O(3)	1.897(3)		
V(2)−O(4)	1.915(3)	V(5)−O(12)	1.596(3)
V(2)−O(7)	1.962(3)	V(5)−O(11)	1.822(3)
V(2)−O(6)	1.988(2)	V(5)−O(9)	1.829(3)
V(2)−V(5)	3.0424(8)	V(5)−O(6)	1.906(2)
Σs[V(1)−O] = 4.36		V(5)−O(7)	1.944(2)
		Σs[V(1)−O] = 4.94	
V(3)−O(8)	1.594(3)		
V(3)−O(4)#1	1.708(3)		
V(3)−O(6)	1.916(3)		
V(3)−O(11)#2	1.946(2)		
V(3)−O(9)	2.055(3)		
V(3)−V(5)	2.9908(8)		
Σs[V(1)−O] = 4.86			

O(1)−V(1)−O(2)	110.20(15)	O(10)−V(4)−O(7)	109.27(13)
O(1)−V(1)−N(2)	125.62(14)	O(3)#3−V(4)−O(7)	96.03(12)
O(2)−V(1)−N(2)	124.16(14)	O(10)−V(4)−O(9)#4	107.93(13)
O(1)−V(1)−N(3)	96.65(13)	O(3)#3−V(4)−O(9)#4	94.92(12)
O(2)−V(1)−N(3)	102.29(14)	O(7)−V(4)−O(9)#4	136.08(11)
N(2)−V(1)−N(3)	74.66(12)	O(10)−V(4)−O(11)	104.01(12)
O(1)−V(1)−N(1)	97.96(13)	O(3)#3−V(4)−O(11)	149.24(12)
O(2)−V(1)−N(1)	97.87(14)	O(7)−V(4)−O(11)	75.14(10)
N(2)−V(1)−N(1)	74.76(13)	O(9)#4−V(4)−O(11)	73.91(10)
N(3)−V(1)−N(1)	149.18(13)	O(12)−V(5)−O(11)	108.56(12)
O(5)−V(2)−O(3)	108.32(13)	O(12)−V(5)−O(9)	105.95(13)
O(5)−V(2)−O(4)	103.17(13)	O(11)−V(5)−O(9)	100.03(12)
O(3)−V(2)−O(4)	88.88(11)	O(12)−V(5)−O(6)	109.09(12)
O(5)−V(2)−O(7)	108.35(12)	O(11)−V(5)−O(6)	140.38(11)
O(3)−V(2)−O(7)	142.41(12)	O(9)−V(5)−O(6)	81.07(11)
O(4)−V(2)−O(7)	90.64(11)	O(12)−V(5)−O(7)	106.53(12)
O(5)−V(2)−O(6)	104.09(12)	O(11)−V(5)−O(7)	80.55(11)
O(3)−V(2)−O(6)	88.27(11)	O(9)−V(5)−O(7)	145.42(11)
O(4)−V(2)−O(6)	152.07(12)	O(6)−V(5)−O(7)	77.42(10)
O(7)−V(2)−O(6)	75.14(10)	V(4)#1−O(3)−V(2)	176.21(16)
O(5)−V(2)−V(5)	103.42(9)	V(3)#3−O(4)−V(2)	156.73(18)
O(3)−V(2)−V(5)	122.78(8)	V(5)−O(6)−V(3)	102.97(11)
O(4)−V(2)−V(5)	128.13(8)	V(5)−O(6)−V(2)	102.74(12)
O(8)−V(3)−O(4)#1	107.39(14)	V(3)−O(6)−V(2)	131.09(14)
O(8)−V(3)−O(6)	106.63(12)	V(4)−O(7)−V(5)	103.17(12)
O(4)#1−V(3)−O(6)	96.50(12)	V(4)−O(7)−V(2)	133.92(14)
O(8)−V(3)−O(11)#2	103.94(12)	V(5)−O(7)−V(2)	102.32(11)
O(4)#1−V(3)−O(11)#2	95.59(11)	V(5)−O(9)−V(4)#2	145.61(15)
O(6)−V(3)−O(11)#2	141.86(11)	V(5)−O(9)−V(3)	100.53(11)
O(8)−V(3)−O(9)	106.76(13)	V(4)#2−O(9)−V(3)	106.62(12)
O(4)#1−V(3)−O(9)	145.81(12)	V(5)−O(11)−V(3)#4	135.30(14)
O(6)−V(3)−O(9)	75.31(10)	V(5)−O(11)−V(4)	100.54(11)
O(11)#2−V(3)−O(9)	74.45(10)	V(3)#4−O(11)−V(4)	105.01(11)
O(10)−V(4)−O(3)#3	106.70(13)		

[a] Symmetry transformations used to generate equivalent atoms: (#1) $-x+1/2, y-1/2, -z+1/2$; (#2) $-x+3/2, y-1/2, -z+1/2$; (#3) $-x+1/2, y+1/2, -z+1/2$; (#4) $-x+3/2, y+1/2, -z+1/2$.

state syntheses, allows retention of the structural integrity of the organic constituents and promotes "self-assembly" of metastable phases from simple molecular precursors. Finally, the accessibility of a vast parameter space, including stoichiometries, temperature, pressure, pH, fill volume, starting materials, templates, and mineralizers permits significant variations in conditions for the isolation of both molecular complexes and solid-phase materials for a given compositional system.

Such general considerations influence the syntheses of **VOXI-10**−**12**. The preparations exploit the hydrothermal reactions of V_2O_5, 2,2′:6′,2″-terpyridine (terpy), ZnO, and H_2O at 210 °C for various time periods. The material $[V_2O_4(terpy)_2]_3[V_{10}O_{28}]\cdot 2H_2O$ (**VOXI-10**) is isolated as the major crystalline product after 6 days, while $[VO_2(terpy)][V_4O_{10}]$ (**VOXI-11**) and $[V_9O_{22}(terpy)_3]$ (**VOXI-12**) are formed as a mixture of products after 8 days. Curiously, while it is absent in the products, ZnO is required for the syntheses of all three products. Attempts to improve yields and to obtain monophasic materials by varying stoichiometries, temperatures, and other reaction parameters proved to be unsuccessful. It is noteworthy that both **VOXI-11** and **VOXI-12** are mixed valence materials, as suggested by charge-balance requirements and by the intense coloration of the crystals. In common with other hydrothermal preparations,[46]

Table 4. Selected Bond Lengths (Å), Valence Sums, and Angles (deg) for $[V_9O_{22}(terpy)_3]$ (**VOXI-12**)[a]

V(1)−O(3)	1.621(2)	V(4)−O(10)	1.607(2)
V(1)−O(2)	1.624(2)	V(4)−O(11)	1.687(2)
V(1)−O(1)	1.8294(19)	V(4)−O(9)	2.0413(19)
V(1)−O(4)	1.8613(19)	V(4)−N(3)	2.106(2)
∑s[V(1)−O] = 5.07		V(4)−N(1)	2.110(2)
		V(4)−N(2)	2.162(2)
V(2)−O(5)	1.6033(19)	∑s[V(4)−L] = 4.71	
V(2)−O(4)	1.722(2)		
V(2)−O(7)	1.7521(18)	V(5)−O(12)	1.586(3)
V(2)−O(6)	1.7932(5)	V(5)−O(11)#2	1.916(2)
∑s[V(2)−O] = 5.14		V(5)−O(11)	1.916(2)
		V(5)−N(4)	2.106(2)
V(3)−O(8)	1.6170(19)	V(5)−N(4)#2	2.106(2)
V(3)−O(9)	1.6656(19)	V(5)−N(5)	2.163(3)
V(3)−O(1)#1	1.7680(19)	∑s[V(5)−L] = 4.29	
V(3)−O(7)	1.8356(19)		
∑s[V(3)−O] = 5.13			

O(3)−V(1)−O(2)	108.43(11)	N(3)−V(4)−N(1)	147.90(9)
O(3)−V(1)−O(1)	111.78(10)	O(10)−V(4)−N(2)	163.93(11)
O(2)−V(1)−O(1)	113.12(10)	O(11)−V(4)−N(2)	92.16(11)
O(3)−V(1)−O(4)	108.52(10)	O(9)−V(4)−N(2)	76.22(8)
O(2)−V(1)−O(4)	110.04(10)	N(3)−V(4)−N(2)	73.97(9)
O(1)−V(1)−O(4)	104.82(9)	N(1)−V(4)−N(2)	73.94(9)
O(5)−V(2)−O(4)	108.81(10)	O(12)−V(5)−O(11)#2	98.56(8)
O(5)−V(2)−O(7)	109.36(10)	O(12)−V(5)−O(11)	98.56(8)
O(4)−V(2)−O(7)	107.62(9)	O(11)#2−V(5)−O(11)	162.89(15)
O(5)−V(2)−O(6)	109.78(8)	O(12)−V(5)−N(4)	105.82(6)
O(4)−V(2)−O(6)	109.47(7)	O(11)#2−V(5)−N(4)	87.11(8)
O(7)−V(2)−O(6)	111.73(7)	O(11)−V(5)−N(4)	88.24(8)
O(8)−V(3)−O(9)	109.34(10)	O(12)−V(5)−N(4)#2	105.82(6)
O(8)−V(3)−O(1)#1	110.95(10)	O(11)#2−V(5)−N(4)#2	88.24(8)
O(9)−V(3)−O(1)#1	108.37(10)	O(11)−V(5)−N(4)#2	87.11(8)
O(8)−V(3)−O(7)	109.98(9)	N(4)−V(5)−N(4)#2	148.35(13)
O(9)−V(3)−O(7)	107.53(9)	O(12)−V(5)−N(5)	180.000(1)
O(1)#1−V(3)−O(7)	110.59(9)	O(11)#2−V(5)−N(5)	81.44(8)
O(10)−V(4)−O(11)	103.90(13)	O(11)−V(5)−N(5)	81.44(8)
O(10)−V(4)−O(9)	87.74(11)	N(4)−V(5)−N(5)	74.18(6)
O(11)−V(4)−O(9)	168.34(10)	N(4)#2−V(5)−N(5)	74.18(6)
O(10)−V(4)−N(3)	104.41(10)	V(3)#1−O(1)−V(1)	168.35(13)
O(11)−V(4)−N(3)	91.47(9)	V(2)−O(4)−V(1)	149.32(13)
O(9)−V(4)−N(3)	86.25(8)	V(2)#3−O(6)−V(2)	180.0
O(10)−V(4)−N(1)	106.18(10)	V(2)−O(7)−V(3)	148.08(12)
O(11)−V(4)−N(1)	90.51(9)	V(3)−O(9)−V(4)	160.19(11)
O(9)−V(4)−N(1)	85.43(8)	V(4)−O(11)−V(5)	166.52(16)

[a] Symmetry transformations used to generate equivalent atoms: (#1) $-x + 1/2, -y - 1/2, -z + 1$; (#2) $-x + 1, y, -z + 1/2$; (#3) $-x + 1/2, -y + 1/2, -z + 1$.

it is likely that the nitrogenous ligand serves as the reducing agent in these reactions.

As shown in Figure 1, the structure of $[V_2O_4(terpy)_2]_3[V_{10}O_{28}]\cdot 2H_2O$ consists of discrete binuclear cations $[V_2O_4(terpy)_2]^{2+}$ and $\{V_{10}O_{28}\}^{6-}$ one-dimensional chains. The V(V) sites of the cation exhibit distorted octahedral geometry through coordination to a terminal oxo group, two bridging oxo groups, and the three nitrogen donors of a terpyridyl ligand. Since the nitrogen donors must adopt a *meridional* orientation about the metal center, the oxo groups must occupy the opposite triangular face. One consequence of this geometric constraint is the unusual anti coplanar geometry of the $[V_2O_4]^{2+}$ core.[47] The bridging oxo groups link in an asymmetric fashion with long and short V−O interactions that average 2.35 and 1.66 Å, respectively. The long V−O distance is trans to the terminal oxo group, as anticipated. Consequently, the binuclear cation may be described as two weakly associated $\{VO_2(terpy)\}^{1+}$ square pyramids, with a long additional axial bond.

The $\{V_{10}O_{28}\}^{6-}$ subunit is a one-dimensional chain of $\{V_4O_{12}\}^{4-}$ rings linked through corner-sharing $\{VO_4\}^{2-}$ tetrahedra. The cyclic eight-membered ring structure of the $\{V_4O_{12}\}^{4-}$ subunit is essentially identical to that previously observed in $(Bu_4N)_3HV_4O_{12}$.[48] The vanadium sites exhibit distorted tetrahedral geometries defined by two terminal oxo groups with an average $V-O_t$ bond distance of 1.628(5) Å and two bridging oxo groups with $V-O_b$ of 1.839(5) Å and a second tetrahedral geometry defined by one terminal oxo group at 1.608(3) Å and three bridging oxo groups at an average distance of 1.753(5) Å. While a number of one-dimensional chain structures of vanadium are known,[49−55] the $\{V_4O_{12}\}^{4-}$ building block is unique to **VOXI-10**. On the other hand, this cluster is a common structural motif of molecular species.[56,57]

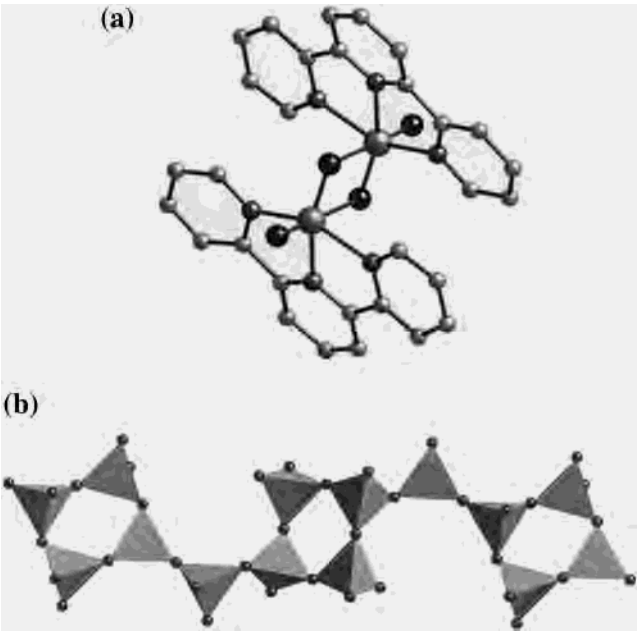

Figure 1. (a) View of the binuclear $[V_2O_4(terpy)_2]^{2+}$ cation of $[V_2O_4(terpy)_2]_3[V_{10}O_{28}]\cdot 2H_2O$ (**VOXI-10**). (b) Polyhedral representation of the anionic vanadium oxide chain of **VOXI-10**.

One other example of a one-dimensional vanadium oxide chain with coordinated organonitrogen ligands has been reported, $[V_9O_{21}(bipy)_4]$.[33] As shown in Figure 2, the structure consists of $\{V_7O_{19}\}^{4-}$ chains decorated with $\{VO(bipy)_2\}^{2+}$ subunits linked through bridging oxo groups. The chain is constructed of corner-sharing $\{VO_4\}$ tetrahedra, $\{VO_5\}$ square pyramids, and $\{VO_2N_4\}$ octahedra. The structure may be viewed as two chains of corner-sharing $\{VO_4\}$ tetrahedra linked by $\{VO_5\}$ square pyramids into a double chain. Every third $\{VO_4\}$ unit enjoys a corner-sharing interaction with a $\{VO_2(bipy)_2\}$ unit that projects outward from the $\{V_7O_{19}\}^{4-}$ ribbon. Valence sum calculations[58] on $[V_9O_{21}(bipy)_4]$ confirm that the tetrahedral sites are V(V) while the square pyramidal and octahedral sites are V(IV). In contrast, all the vanadium centers of **VOXI-10** are in the +5 oxidation state. The unusual structures of **VOXI-**

(47) Plass, W. *Angew. Chem., Int. Ed. Engl.* **1996**, *35*, 627.
(48) Fuchs, J.; Mahjour, S.; Pickardt, J. *Angew. Chem., Int. Ed. Engl.* **1976**, *15*, 374.
(49) Evans, H. T., Jr. *J. Am. Chem. Soc.* **1960**, *114*, 257.
(50) Ganne, M.; Piffard, Y.; Touroux, M. *Can. J. Chem.* **1974**, *52*, 3539.
(51) Björnberg, A.; Hedman, B. *Acta Chem. Scand.* **1977**, *A31*, 579.
(52) Dubois, S.; Souchay, P. *Ann. Chim. (Paris)* **1948**, *3*, 105.
(53) Sedlacek, P.; Dornberger-Schiff, K. *Acta Crystallogr.* **1965**, *18*, 407.
(54) Hawthorne, F. C.; Calvo, C. *J. Solid State Chem.* **1977**, *22*, 157.
(55) Aschwanden, S.; Schmalle, H. W.; Reller, A.; Oswald, H. R. *Mater. Res. Bull.* **1993**, *28*, 45.
(56) Day, V. W.; Klemperer, W. G.; Yagosaki, A. *Chem. Lett.* **1990**, 1267.
(57) Zhang, Y.; Zapf, P.; Meyer, L. M.; Haushalter, R. C.; Zubieta, J. *Inorg. Chem* **1997**, *36*, 2159.
(58) Brown, I. D.; Alternatt, D. *Acta Crystallogr.* **1985**, C*41*, 244.

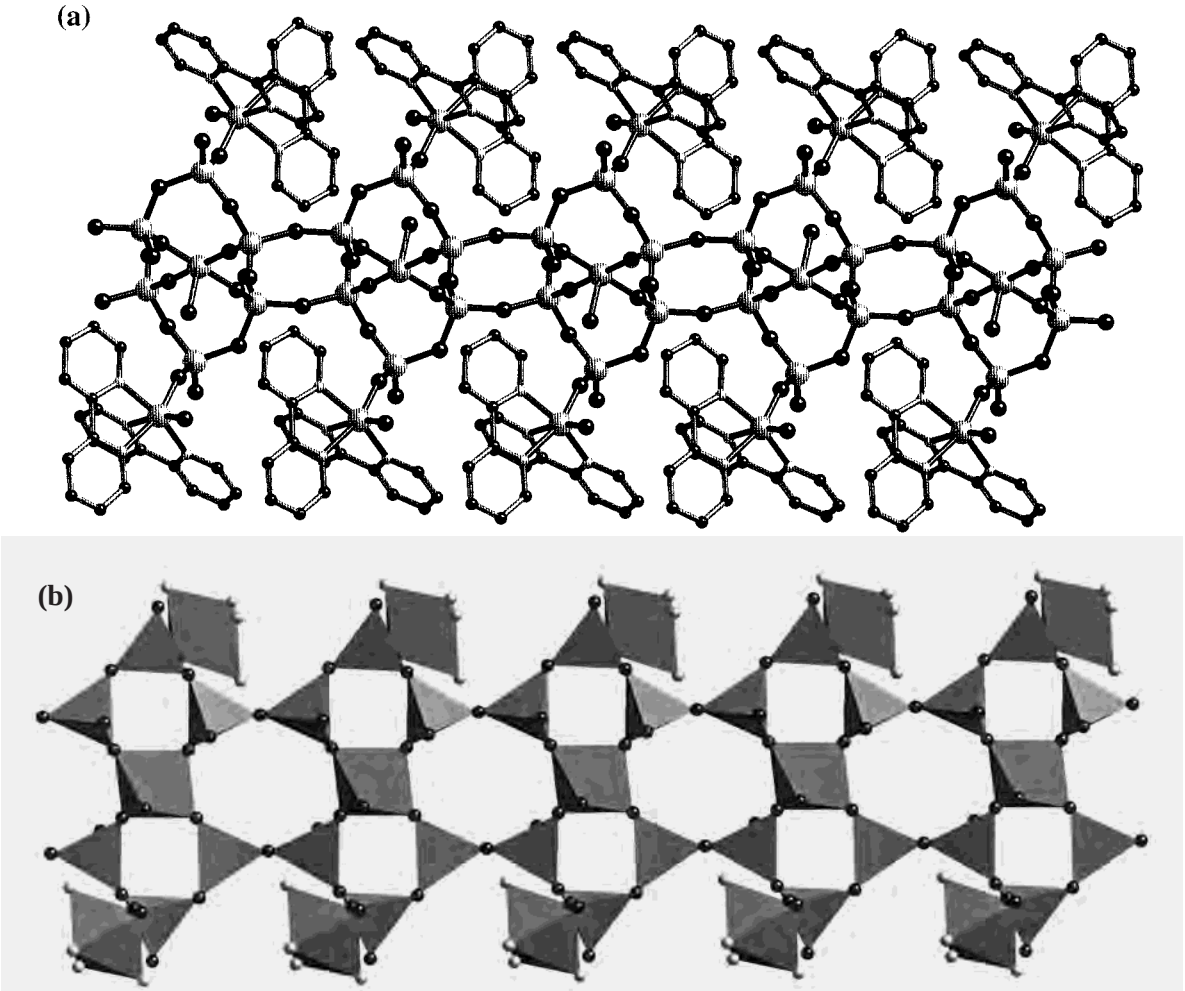

Figure 2. (a) View of the structure of $[V_9O_{21}(bipy)_4]$.[33] (b) Polyhedral representation of the vanadium oxide chain structure of $[V_9O_{21}(bipy)_4]$.

10 and $[V_9O_{21}(bipy)_4]$ and the absence of common structural motifs suggest that the architectures of phases of the V−O-organonitrogen family will display considerable diversity and will exhibit strong dependence on synthetic conditions. This expectation is realized in the structure of $[VO_2(terpy)][V_4O_{10}]$ (**VOXI-11**).

The structure of **VOXI-11**, shown in Figure 3, consists of discrete $[VO_2(terpy)]^{1+}$ cations and $[V_4O_{10}]^{1-}$ two-dimensional networks. In contrast to the structure of **VOXI-10**, the $[VO_2(terpy)]^{1+}$ unit is mononuclear, with no long-range V−O interactions providing bridging into binuclear units. As shown in Table 5, a comparison of the geometries of the $[VO_2(terpy)]^{1+}$ subunits of **VOXI-10** and **VOXI-11** demonstrates that both are intermediate structures considerably distorted from the square pyramidal and trigonal bipyramidal limits.[59]

The structure of the $[V_4O_{10}]^{1-}$ network of **VOXI-11** is illustrated in Figure 3b. The structure may be described as undulating ribbons of edge-sharing square pyramids linked to adjacent ribbons through corner-sharing interactions. It is noteworthy that each ribbon is constructed of two double chains of corner-sharing polyhedra, one with the terminal oxo group of every square pyramid oriented to one surface of the layer and the second with all terminal oxo groups directed to the other surface of the network. One consequence of this arrangement is the number of distinct sites within the layer. The V(5) site exhibits edge-sharing interactions with three polyhedra of the anti oriented chain of the ribbon and corner-sharing interactions with two square pyramids within the chain. The V(3) and V(4) sites exhibit cis edge-sharing with two polyhedra of the anti chain of the same ribbon, corner-sharing to two square pyramids within the chain, and corner-sharing to an adjacent ribbon. The V(2) site enjoys edge-sharing to a single square pyramid of the anti chain of the same ribbon, corner-sharing to two polyhedra of the same chain, and corner-sharing to two square-pyramids of an adjacent ribbon. Alternatively, the structure may be regarded as a defected network in which every third site is vacant along the *a* direction, while along the *b* direction, the vacancies alternate on every second site in one chain followed by every fourth site in two adjacent chains. The network structure of **VOXI-11** is quite distinct from that of the V_2O_5 layer structure[60] and those of previously reported organically templated two-dimensional vanadium oxides,[17−29] as well as ammonium templated phases.[61,62] As shown in Figure 4, the structures of V_2O_5, LiV_2O_5,[63] and $(NMe_4)V_4O_{10}$ may be considered defect structures based on the $VO_2\cdot(^1/_2)H_2O$ structure.[64] The structures of V_2O_5, LiV_2O_5, and $(NMe_4)V_4O_{10}$ exhibit a similar pattern of polyhedral vacancies in the layer, running

(59) (a) Muetterties, E. L.; Guggenberger, M. R. *J. Am. Chem. Soc.* **1974**, *96*, 1748. (b) Addison, A. W.; Rao, T. N.; Reejijk, K.; Rijn, J.; Verschoor, G. C. *J. Chem. Soc., Dalton Trans.* **1984**, 1349.

(60) Enjalbert, R.; Galy, J. *Acta Crystallogr.* **1986**, *C42*, 1467.

(61) Huang, S. D.; Shan, Y. *Chem. Commun.* **1998**, 1069.

(62) A comprehensive review of the structural chemistry of vanadium oxide phases is provided in the following. Zavalij, P. Y.; Whittingham, M. S. *Acta Crystallogr.* **1999**, *B55*, 627.

(63) Cava, R. J.; Santoro, A.; Murphy, D. W.; Zahurak, S. M.; Fleming, R. M. *J. Solid State Chem.* **1986**, *65*, 63.

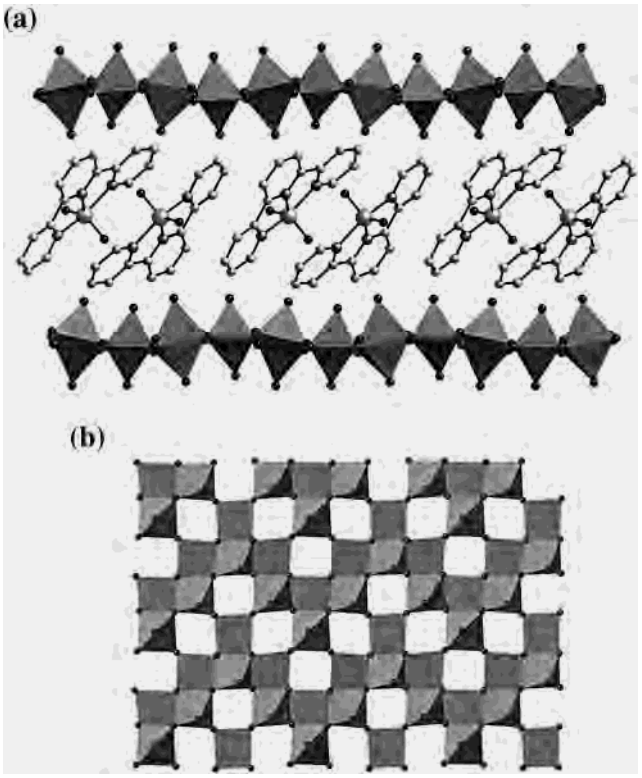

Figure 3. (a) View of the structure of $[VO_2(terpy)][V_4O_{10}]$ (**VOXI-11**) parallel to $[V_4O_{10}]^{1-}$ layers. (b) Polyhedral representation of the $[V_4O_{10}]^{1-}$ network of **VOXI-11** normal to the *ab* plane.

in parallel diagonal lines in the perspective of the figure. The structures differ only in the relative up/down orientations of the square pyramidal $\{VO_5\}$ polyhedra with respect to the oxide plane. In contrast, **VOXI-11** exhibits a zigzag pattern of vacancies as a consequence of its distinctive polyhedral connectivity pattern.

Charge balance considerations and the deep coloration of the crystals of **VOXI-11** indicate a mixed valence species. The charge of the $[V_4O_{10}]^{-1}$ network results in a formalism of one V(IV) and three V(V) sites. The valence sum calculations of Table 3 suggest that the electron is not totally delocalized but is associated with the V(2) center. It is noteworthy that sites V(3), V(4), and V(5) form a linear triad of edge-sharing square pyramids, while the V(1) site is uniquely sited to edge-share with the central V(5) site of the triad and corner-share to the V(3) and V(4) sites that serve as the termini of the triad.

The structures of **VOXI-10** and **VOXI-11** fail to incorporate the terpy ligand into the extended vanadium oxide substructure, rather localizing the ligand in the molecular cationic components. In contrast, the prototypical materials $[V_9O_{21}(bipy)_4]$ and $[V_3O_7(o\text{-phen})]$ both exhibit direct bonding of the ligand to the oxide scaffolding. Consequently, it was anticipated that the terpyridine ligand should also coordinate to the oxide substructure.

The structure of $[V_9O_{22}(terpy)_3]$ (**VOXI-12**), shown in Figure 5, provides the structural prototype for incorporation of the terpyridyl ligand into the oxide structure. The structure of **VOXI-12** consists of stepped vanadium oxide layers with the terpyridyl groups projecting into the interlamellar region. The layer is constructed of exclusively corner-sharing $\{VO_4\}$ tetrahedra and $\{VO_3N_3\}$ octahedra.

The network may be described in terms of two characteristic motifs, 12-membered cyclic $\{V_6O_6\}$ units constructed of corner-sharing $\{VO_4\}$ tetrahedra and linear trinuclear $\{V_3O_5(terpy)_3\}$ subunits. Each hexanuclear ring links to two adjacent rings to form a one-dimensional daisy chain. These chains are linked through the terminal vanadium sites of the trinuclear units into the two-dimensional network. One consequence of this connectivity is the appearance of a second cyclic motif constructed from 10 $\{VO_4\}$ tetrahedra and 6 $\{VO_3N_3\}$ octahedra, giving rise to a $\{V_{16}O_{16}\}$ ring. The terpyridyl ligands are oriented about the octahedral vanadium sites to project the terminal rings into the interlamellar regions above and below the oxide layer. However, the central ring must then be accommodated within the layer, necessitating considerable expansion of ring dimensions to encircle the sterically demanding organic component. Consequently, the influence of the organic subunit on the network structure of **VOXI-12** is rather significant.

The structure of **VOXI-12** may be compared to that of the previously reported example of a two-dimensional vanadium oxide incorporating an organonitrogen ligand, $[V_3O_7(o\text{-phen})]$. As shown in Figure 6, the structure of $[V_3O_7(o\text{-phen})]$ is constructed from corner-sharing $\{VO_4\}$ tetrahedra and $\{VO_3N_2\}$ square pyramids. The structure may be described as puckered $\{VO_4\}$ chains linked by $\{VO_3N_2\}$ square pyramids into a two-dimensional network. It is noteworthy that the steric demands of the *o*-phenanthroline ligand necessitate some ring expansion in the network, which results in an eight polyhedral connect $\{V_8O_8\}$ ring constructed from six $\{VO_4\}$ tetrahera and two $\{VO_3N_2\}$ square pyramids. It is noteworthy that the sterically more demanding terpyridyl ligand generates a 16 polyhedral connect ring in **VOXI-12**.

Both $[V_3O_7(o\text{-phen})]$ and **VOXI-12** are mixed valence materials. In the case of $[V_3O_7$ (*o*-phen)], the V(IV) site is the square pyramidal $\{VO_3N_2\}$, that is, the vanadium site coordinated to the ligand. In the case of **VOXI-12**, valence sum calculations establish the tetrahedral sites as V(V), while the ligated octahedral sites exhibit valence sums of 4.7 for the terminal vanadium centers and 4.3 for the central site, suggesting that the electron is not totally localized on the V(5) site. A common feature of the structures of $[V_9O_{21}(bipy)_4]$, $[V_3O_7(o\text{-phen})]$, and **VOXI-12** is the reduction of vanadium sites coordinated to the ligand to the V(IV) oxidation state. While it is tempting to speculate that reduction to the V(IV) state occurs concomitantly to incorporating the ligand at the reduced site, the small number of structures available to date precludes any conclusion based on this observation. Certainly, the structures of **VOXI-10** and **VOXI-11** demonstrate that ligation under hydrothermal conditions to the molecular cationic subunit does not result in reduction of the vanadium centers. As more examples such vanadium oxide ligand hybrids are characterized, the consequences of ligand incorporation into the oxide substructure on the oxidation states of the metal should begin to emerge.

Conclusions

The isolation of **VOXI-10**−**12** confirms our previous observation[30] that hydrothermal synthesis provides a simple single-step route to a new class of inorganic solid-state materials, incorporating organonitrogen ligands into vanadium oxide substructures. It is apparent that the introduction of an organic component may have a dramatic influence on the oxide microstructure, albeit an often unpredictable one. Predictability is limited by the structural complexity of such hybrid systems. For instance, the occurrence of different vanadium coordination

(64) Hagrman, D.; Zubieta, J.; Warren, C. J.; Meyer, L. M.; Treacy, M. M. J.; Haushalter, R. C. *J. Solid State Chem.* **1998**, *138*, 178.

Table 5. Idealized Angles (deg) for ML_5 Complexes and Observed Angles for the $\{VO_2(terpy)\}$ Sites of $[V_2O_4(terpy)_2]_3[V_{10}O_{28}]$ (**VOXI-10**) and $[VO_2(terpy)][V_4O_{10}]$ (**VOXI-11**)

	shape determining δ' angles (e_3, e_1, and e_2)	δ angles (a_2, a_5, and remaining angles)
ideal trigonal bipyramid	53.1, 53.1, 53.1	101.5, 101.5, 101.5, 101.5, 101.5, 101.5
VOXI-10	19.8, 45.1, 73.9	85.1, 83.9, 124.7, 109.8, 125.3, 110.7
VOXI-11	30.3, 47.6, 72.3	97.4, 105.5, 121.2, 108.4, 122.6, 100.4
ideal square pyramid	0, 75.7, 75.7	75.7, 75.7, 119.8, 119.8, 119.8, 119.8

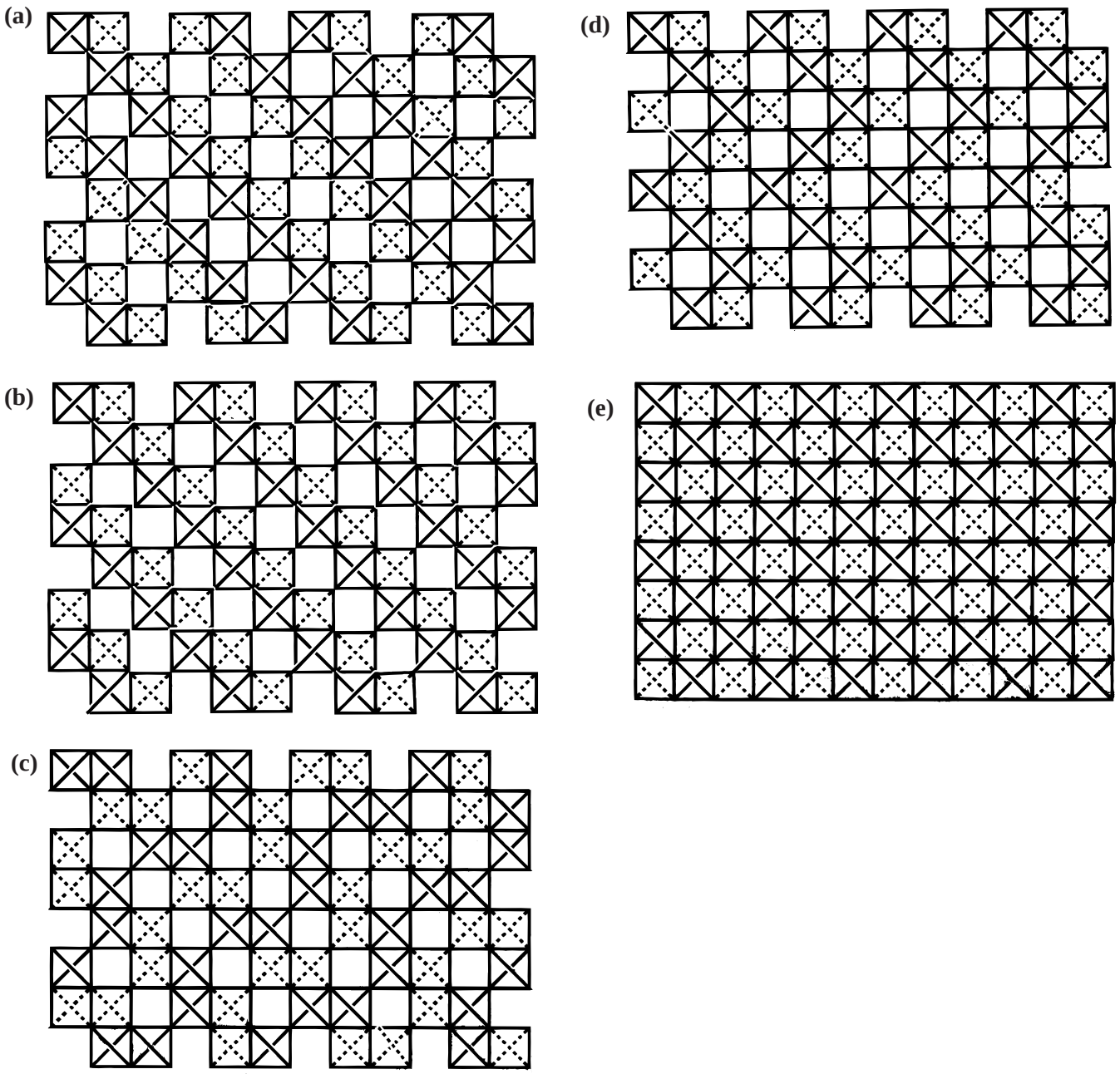

Figure 4. Schematic representations of the layer structures of (a) V_2O_5,[60] (b) LiV_2O_5,[63] (c) $(NMe_4)V_4O_{10}$,[62] (d) $[VO_2(terpy)][V_4O_{10}]$, and (e) $VO_2 \cdot 0.5\ H_2O$.[64]

geometries and the accessibility of more than one vanadium oxidation state give rise to an unusually varied structural chemistry for vanadium oxide systems. Vanadium−oxygen polyhedra with tetrahedral, octahedral, distorted octahedral, square pyramidal, and trigonal bipyramidal geometries are typically observed. Polyhedral connectivity into oligomers or extended structures may occur through combinations of edge-, corner-, and face-sharing interactions. The introduction of organic components allows further structural modification through templating, passivation of the surface of a growing oxide to restrict spatial extension, and communication of structural information in extended solids.

The passivation of the oxide to favor lower dimensional structures is represented by the one-dimensional structure of **VOXI-10**. The tendency of vanadium oxide to form two-dimensional inorganic substructures has been disrupted through introduction of the bulky organic ligand, although in this case structural modification occurs not through direct ligation of the

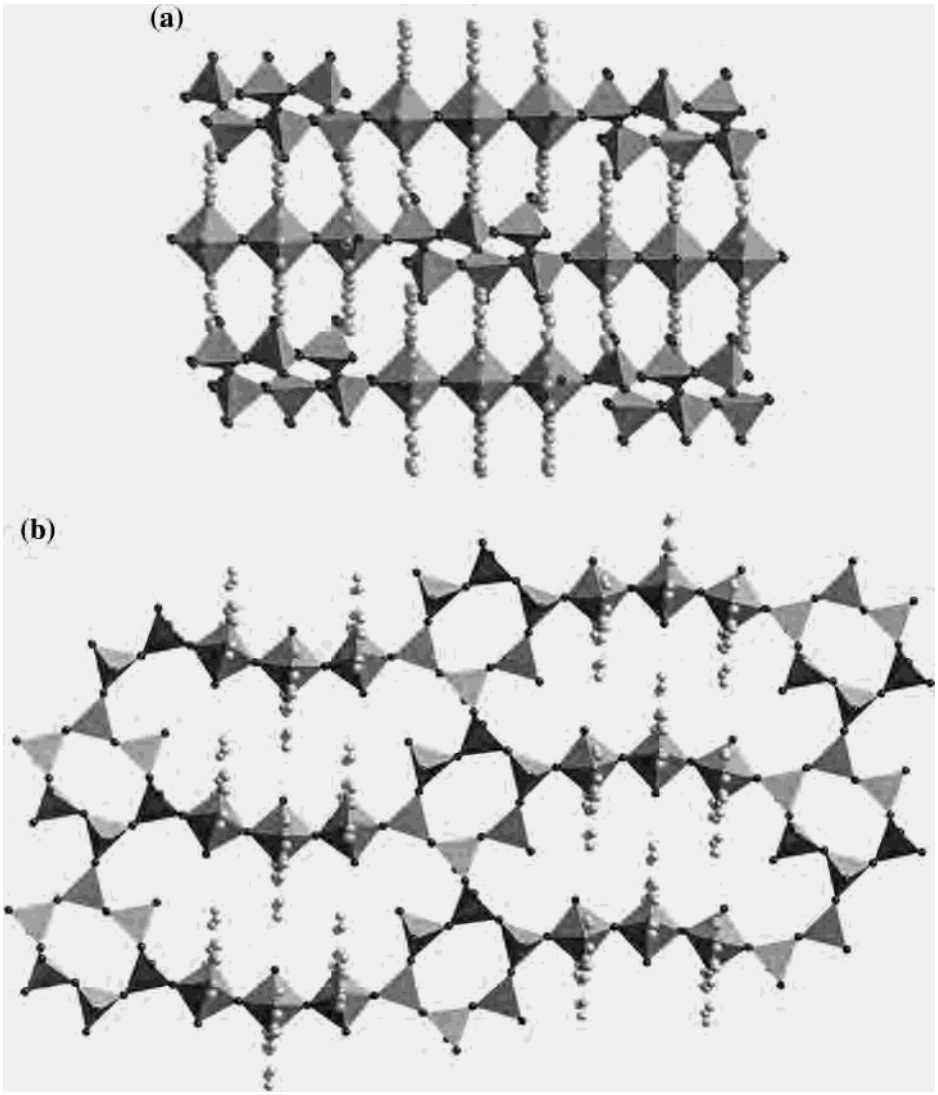

Figure 5. (a) View of the structure of $[V_9O_{22}(terpy)_3]$ (**VOXI-12**) parallel to the vanadium oxide layers. (b) Polyhedral representation of the network structure of **VOXI-12**.

ligand to the oxide substructure but through formation of a bulky charge-compensating and space-filling cation, $[V_2O_4(terpy)_2]^{2+}$. In contrast, **VOXI-11** presents a mixed valence vanadium oxide layer structure, related both compositionally and structurally to the V_2O_5 starting material. The degree of reduction [V(IV)/V(V)] and condensation, in the sense of V/O ratio and relative amounts of edge-sharing versus corner-sharing polyhedral connectivities within the layers, is reflected in the charge per volume ratio of the cationic intralamellar coordination complex. Thus, the average oxidation state of the vanadium sites in the layer is related to the structural distortion from the prototypical, fully oxidized V_2O_5 structure. The range of average oxidation states associated with the organically templated structures is thus extensive: 4.83 for $[NMe_4]_5[V_{18}O_{46}]$,[26] 4.75 for **VOXI-11**, 4.60 for $[Cu(en)_2][V_6O_{14}]$,[30] and 4.33 for $[Cu(en)_2]_2[V_{10}O_{25}]$.[30] Furthermore, the extensive edge- and corner-sharing of the vanadium polyhedra in these hybrid materials appears to influence electron−electron interactions confined within the layer.

The material $[V_9O_{22}(terpy)_3]$ (**VOXI-12**) is unusual in that the ligand is incorporated directly into the vanadium oxide substructure. Comparison to the only other example of a two-dimensional vanadium oxide−organonitrogen ligand phase, $[V_3O_7(phen)]$,[34] reveals that average oxidation states are 4.89 for **VOXI-12** and 4.67 for $[V_3O_7(phen)]$. However, for these ligated hybrid network materials, the oxidation state does not appear to reflect the degree of condensation and structural similarity to V_2O_5 but rather to be related to the subtle interplay of ligand steric requirements and redox potentials with the ability of the network connectivity pattern to accommodate the geometric constraints of the ligand.

The materials **VOXI-10**−**12** are metastable structures whose assembly is controlled by kinetic factors. In the cases of **VOXI-10** and **VOXI-12**, the presence of preformed building blocks in solution at some stage in the nucleation process is implicated by the presence of $\{V_4O_{12}\}^{4-}$ and $\{V_6O_{18}\}^{6-}$ "clusters" embedded in the extended structures. For **VOXI-11**, the edge-sharing ribbons of vanadium square pyramids may arise from preferential dissolution of V_2O_5 parallel to the direction of the vertex-linked ribbons.

It is also noteworthy that while factors such as stoichiometry, ligand geometry and uptake, dissolution of the oxide starting material, pH, temperature, and time interact in dictating the rate of nucleation and crystallization of the oxide, redox chemistry is an additional determinant. The hydrothermal chemistry of such oxides is controlled in part by the reduction of V_2O_5 in the medium, which is a consequence of reaction with the organic substituent.

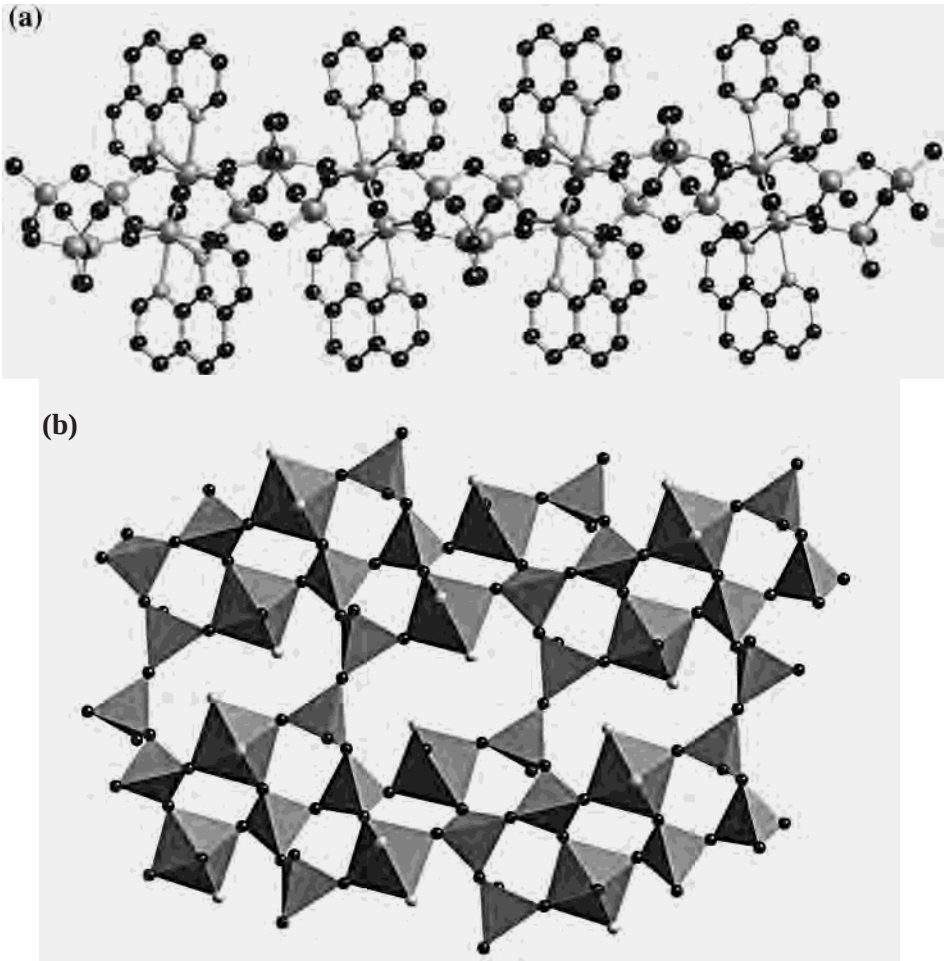

Figure 6. (a) View of the structure of $[V_3O_7(o\text{-phen})]$ parallel to the oxide plane.[34] (b) Polyhedral representation of the vanadium oxide layer of $[V_3O_7(o\text{-phen})]$.

While the structure-directing and redox roles of the organic substituent in molybdenum and vanadium oxide chemistry is now apparent, predictability of product remains elusive. This observation reflects in part the relative paucity of structures investigated to date. A systematic study of ligand geometries, denticities, steric requirements, tether lengths, and redox potentials remains to be undertaken. Likewise, a systematic variation of reaction conditions, including solvatothermal processes in organic solvents, must be undertaken. Even so fundamental a study as the composition space of a V_2O_5/ligand/H_2O system has yet to be documented.[65] Our initial essays into these issues will be reported in subsequent publications in this series.

Acknowledgment. This work was supported by a grant from the National Science Foundation, CHE-9987471.

Supporting Information Available: X-ray crystallographic files, in CIF format, for the structure determinations of **VOXI-10**, **VOXI-11**, and **VOXI-12**; ORTEP views of the structures, showing 50% thermal ellipsoids. This material is available free of charge via the Internet at http://pubs.acs.org.

IC991473D

(65) On the other hand, such studies have been reported for CdO, Nb_2O_5/$(HF)_x$·pyridine/H_2O. Halasymani, P. S.; Heier, K. R.; Norquist, A. J.; Stern, C. L.; Poeppelmeier, K. R. *Inorg. Chem.* **1998**, *37*, 369.